Chemistry–A European Journal
Research Article
doi.org/10.1002/chem.202403454
Chemistry Europe
European Chemical Societies Publishing
www.chemeurj.org

# Sonodynamic Cancer Therapy by Mn(I)-tricarbonyl Complexes via Ultrasound-triggered CO Release and ROS Generation

Ashish Kumar Yadav,[a] Virendra Singh,[b] Sagar Acharjee,[a] Sukanta Saha,[c] Rajesh Kushwaha,[a] Arnab Dutta,[c] Biplob Koch,*[b] and Samya Banerjee*[a]

A novel ferrocene conjugated Mn(I)-tricarbonyl complex *viz* [Mn(Fc-tpy)(CO)$_3$Br] (**Mn2**) where, Fc-tpy = 4′-ferrocenyl-2,2′:6′,2″-terpyridine was synthesized and fully characterized along with its non-ferrocene analog [Mn(Ph-tpy)(CO)$_3$Br] Ph-tpy = 4′-phenyl-2,2′:6′,2″-terpyridine (**Mn1**) for ultrasound (US) activated anticancer applications. The X-ray structure of **Mn2** confirmed its distorted octahedral geometry. **Mn1** and **Mn2**, for the first time, showed US-triggered release of CO and ROS generation ($^1O_2$ and ·OH) in an aqueous solution from any Mn(I)-tricarbonyl complexes, indicating its potential for synergetic CO gas therapy and sonodynamic therapy. The above-mentioned in-solution chemistry was successfully translated into *in vitro* cellular models. These complexes showed unprecedented US-triggered toxicity against T-cell lymphoma and human breast cancer cells ($IC_{50}$ for **Mn2** < 1 μM) while were minimally toxic without US or against normal spleen and human embryonic kidney cells. **Mn2** was ca. 12 fold more anticancer active than **Mn1**, indicating that the ferrocene conjugation augmented the US sensitivity. The apoptotic sonotoxicity of **Mn2** was due to US-promoted mitochondrial depolarization via ROS generation and CO release. The apoptosis was triggered by caspase 3 activation. This is the first report of Mn(I)-tricarbonyl-based sonosensitizers for cancer SDT. Overall, this study, for the first time, establishes the effectiveness of 3d metal carbonyls in SDT.

## Introduction

In recent years, Re(I) and Mn(I) tricarbonyl complexes have emerged as promising candidates for anticancer activity.[1–8] Most of them are extensively used for photoactivated cancer therapy (PACT).[1–6] These metal-carbonyl complexes generate reactive oxygen species (ROS) and release carbon monoxide (CO) upon light irradiation.[1–6] This dual action, ROS-induced oxidative stress, and CO-disrupted mitochondrial function, are responsible for their anticancer activity.[1–4] However, light's limited tissue penetration depth hinders their therapeutic applications.[9–12] To overcome this limitation, ultrasound (US) has recently attracted interest as a potential alternative to light for activating these metal-carbonyls.[13,14] Unlike light, the US offers superior tissue penetration, reaching depths up to 10 cm within tumors.[11–13] Due to this advantage, US-driven sonodynamic therapy (SDT) is emerging in anticancer research.[9–14] Metal complexes with rich excited state properties are now being actively explored for SDT applications with positive outcomes.[13,14] Our recent research underscores the efficacy of US in achieving therapeutic anticancer effects from Re(I)-tricarbonyl complexes.[13,14] These findings pave the way for developing novel US-responsive metal-carbonyls, which could provide anticancer activities via ROS generation and CO-release on US exposure. Although the Mn(I)-tricarbonyls were studied as PACT agents,[4,6,15,16] their efficacy in SDT has been completely unexplored. Mn is bioessential and involved in the functionating of several enzymes such as transferases, oxidoreductases, lyases, etc.[17] So, developing Mn(I)-tricarbonyls as sonosensitizers for SDT might provide a bio-compatible anticancer SDT agent with a dual mode of action. Based on the above hypothesis, we have successfully developed two US-responsive Mn(I)-tricarbonyl complexes viz., **Mn1** and **Mn2** (Figure 1a). Herein, N,N,N moiety will enhance the lipophilicity of the complexes, prompting their cellular uptake. Terpyridine-based ligands are well known for US-induced ROS generation. Therefore, **Mn1** and **Mn2** might also generate ROS for SDT.

[a] *A. Kumar Yadav, S. Acharjee, R. Kushwaha, S. Banerjee*
*Department of Chemistry, Indian Institute of Technology (BHU) Varanasi, Uttar Pradesh 221005, India*
*E-mail: samya.chy@itbhu.ac.in*

[b] *V. Singh, B. Koch*
*Department of Zoology, Institute of Science, Banaras Hindu University, Varanasi, Uttar Pradesh 221005, India*
*E-mail: biplob@bhu.ac.in*

[c] *S. Saha, A. Dutta*
*Department of Chemistry, Indian Institute of Technology Bombay, Mumbai, Maharashtra 400076, India*

*Supporting information for this article is available on the WWW under https://doi.org/10.1002/chem.202403454*

## Results and Discussion

### Synthesis, Characterization, and Stability of Complexes Mn1 and Mn2

**Mn1** and **Mn2** were prepared in 80% to 84% yields from the stoichiometric reaction of [Mn(CO)$_5$Br] with the respective terpyridine ligand in Et$_2$O under reflux condition (Scheme S1).

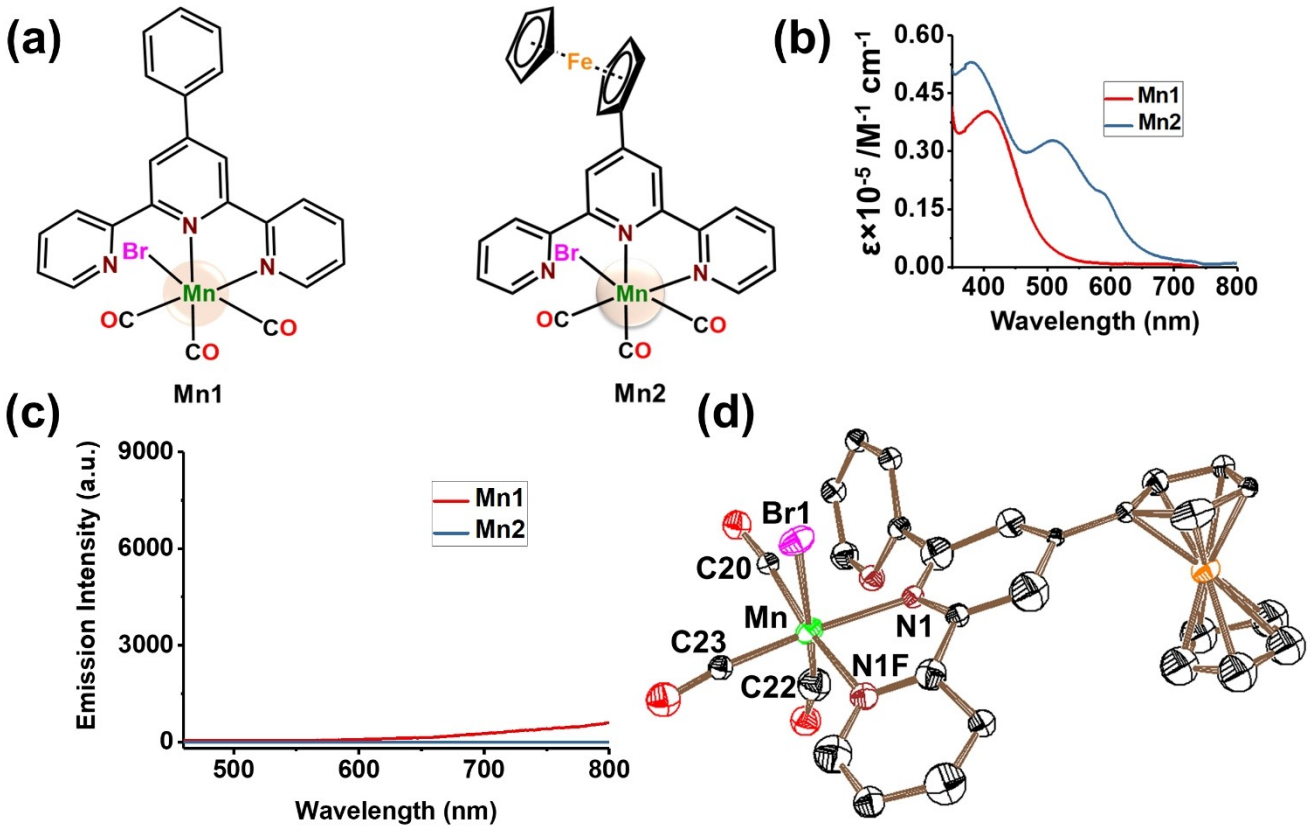


**Figure 1.** (a) Structures of **Mn1** and **Mn2**. (b) Absorption spectra of **Mn1** and **Mn2** in 0.5% DMSO/99.5% PBS (v/v) solution. (c) Emission spectra of **Mn1** and **Mn2** (20 μM each) in acetonitrile [$\lambda_{ex}$ = 410 nm]. (d) Crystal structure of **Mn2** with atom labeling scheme. The thermal ellipsoids are shown at a 50% probability level.

Complexes were characterized using UV-Vis (Figure 1b), emission (Figure 1c), SC-XRD (Figure 1d), HR-MS, multinuclear NMR (Figures S1-S6), and IR (Figures 2a and S7). NMR and elemental analysis data revealed the high purity (>95%) of the complexes. The UV-Vis spectra of **Mn2** in 0.5% DMSO/99.5% PBS (v/v) solution displayed bands between 500–600 nm (Figure 1b). These bands correspond to the Mn(I)-to-ligand charge transfer (MLCT), confirmed by the DFT studies. The emission studies demonstrated the non/very weak emissive behavior of **Mn1** and **Mn2** in acetonitrile (Figure 1c). The FT-IR spectra of the complexes (Figures 2a and S7) showed three distinct IR bands within the 2025–1920 $cm^{-1}$ region, providing evidence for the presence of three facial carbonyl groups within the complexes.[6,16] X-ray structure of **Mn2** revealed a distorted octahedral coordination geometry (Figures 1d and S8). **Mn2** crystallized as an orthorhombic system (Pba2 space group) with 8 molecules per unit cell (Figure S8). Among the three CO, two CO occupied equatorial positions, while the third CO occupied an axial position, trans to the bromide anion. The complete crystallographic data and refinement details are provided in Table S1 and S2. The N1-Mn–N1F angle was characteristically small (77.6°), in line with the previous reports. The bond angles N1-Mn–Br1 (86.8°) and N1F–Mn-Br1 (82.0°) were below 90.0°, indicating that the terpyridine moiety is a little bent towards the axial Br1 (Table S2). The angle Br1-Mn–C20 (88.8°) was lower than 90°, indicating one equatorial CO is bent away from axial CO. The log $P_{o/w}$ values for the complexes **Mn1** and **Mn2** were $-0.8 \pm 0.2$ and $+0.09 \pm 0.03$, respectively. This increase in log $P_{o/w}$ value from **Mn1** to **Mn2** is due to the introduction of ferrocene moiety on the N,N,N-donor ligand in **Mn2**. Complexes were stable in the DMEM cell culture medium (Figures S9 and S10). Further, the stability study of **Mn2** in PBS under dark conditions demonstrated good stability (Figure S11). Thus, these complexes can be used for anticancer applications.[13,16]

## Ultrasound-Induced CO Release

Although earlier investigations indicated that light can release CO from Mn(I)-tricarbonyl complexes,[6,16,18] the same event with US was never achieved. To examine the CO release profile of **Mn1** and **Mn2** upon ultrasound (US) exposure, infrared (IR)

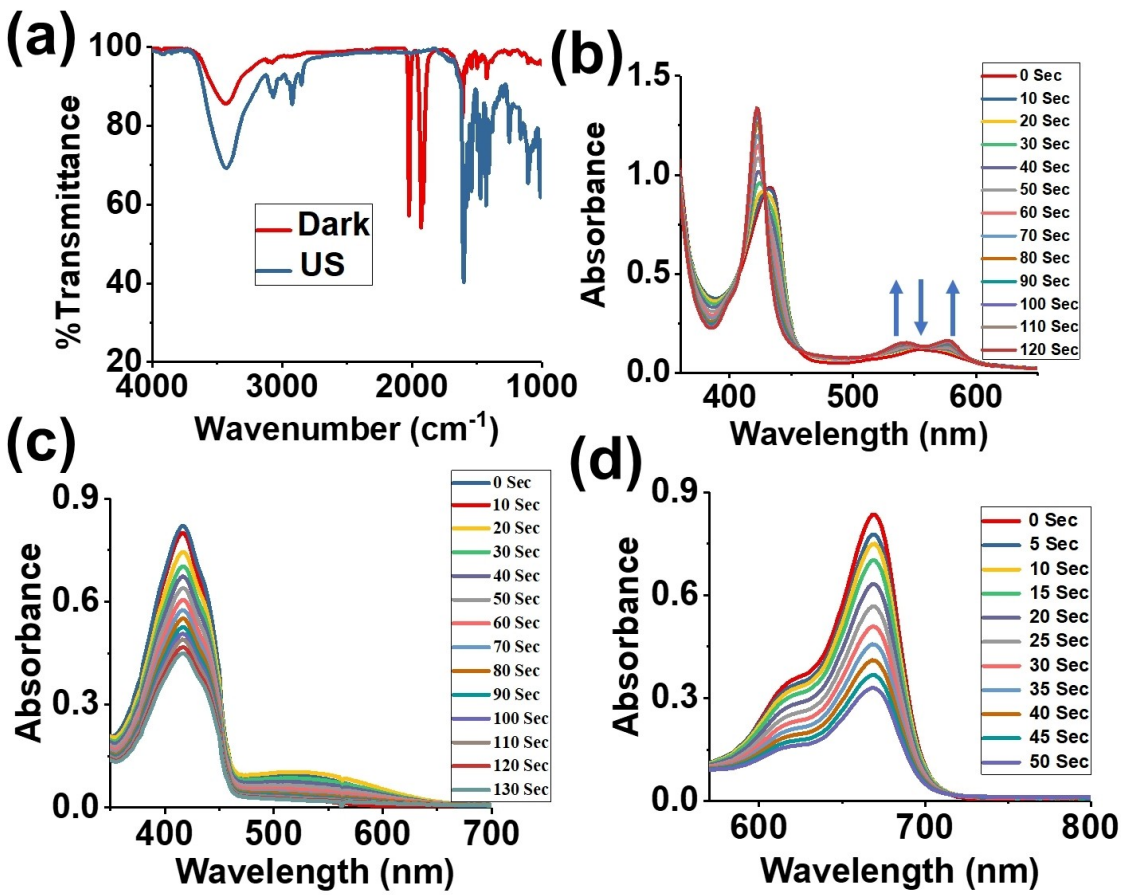


**Figure 2.** (a) FT-IR spectra of **Mn2** before (red trace) and after (blue trace) US exposure (KBR Method). (b) The UV-vis absorption spectra demonstrate CO release from **Mn2** (8 μM) on US (1.0 MHz, 0.3 W/cm$^2$) exposure at different time intervals, as detected with Mb (10 μM). Solvent: 0.5% DMSO/99.5% PBS (v/v) solution (pH = 7). (c) Absorbance changes of DPBF (50 μM) in the presence of **Mn2** (2 μM) + US (1.0 MHz, 0.3 W/cm$^2$) indicating efficient $^1O_2$ formation. Solvent: 0.5% DMSO/99.5% PBS (v/v) solution. (d) Absorbance changes of methylene blue (15 μM) in the presence of **Mn2** (2 μM) + US (1.0 MHz, 0.3 W/cm$^2$) revealing the ·OH generation. Solvent: 0.5% DMSO/99.5% PBS (v/v) solution.

spectroscopy was employed (Figure 2a).[18] The initial IR spectra of **Mn1** and **Mn2** in the solid state revealed characteristic peaks between 2025 and 1920 cm$^{-1}$ corresponding to the presence of three facial carbonyl ligands.[18] Subsequently, a $CHCl_3$ solution of **Mn1**/**Mn2** was subjected to US irradiation (1.0 MHz, 0.3 W/cm$^2$) for 30 minutes, followed by vacuum drying and IR analysis of the residual material. The complete disappearance of the CO bands in the post-US exposed IR spectra (Figure 2a) confirmed the release of all three CO from each complex.[18] This observation aligns with previous studies demonstrating photochemical CO-release from Mn(I)-tricarbonyls.[18] The myoglobin assay was used to further confirm the US-triggered CO release from **Mn1**/**Mn2**.[16,18] Oxymyoglobin ($MbO_2$) initially displayed absorbance at 422 nm.[16,18] Upon reduction, this absorbance shifted to 434 nm due to the formation of deoxymyoglobin.[16,18] By trapping the released CO from **Mn1**/**Mn2**, deoxymyoglobin was converted to Mb-CO, evident by a distinct absorption peak at 422 nm (Figures 2b and S12). Simultaneously, there was a decrease in absorption at 562 nm, while absorption bands at 540 nm and 579 nm exhibited significant increment in intensity, indicating the formation of Mb-CO.[16,18] The increase in absorbance intensity of the Mb-CO bands in the UV-Vis spectra upon US irradiation time confirmed the CO release ability of **Mn1** and **Mn2**.[16,18] It is important to note that this is the first occasion CO release from Mn(I)-tricarbonyls was achieved with the US as the stimulus. This result is highly significant as **Mn1** and **Mn2** might show anticancer effects via CO release under US irradiation.

### In-Solution ROS Generation

In SDT, ROS directly contributes to the cytotoxicity.[11,12,14] Mn(I)-tricarbonyls are known to show phototoxicity via ROS production under light.[19] Therefore, to check the possibility of ROS production by **Mn1**/**Mn2** under US stimulation, their singlet oxygen ($^1O_2$) and ·OH generation was probed with DPBF ($^1O_2$ sensor) and methylene blue (·OH detector), respectively.[20,21] Under US exposure (1.0 MHz, 0.3 W cm$^{-2}$), both, **Mn1** and **Mn2** caused a significant decrease in DPBF absorbance intensity over time (Figures 2c and S13), indicating $^1O_2$ generation by **Mn1**/**Mn2**. Control experiments confirmed that the absorbance

change was not due to US exposure only (Figures 2c and S14). The absorbance of DPBF + **Mn1/Mn2** remained unchanged in the absence of US (Figures S15 and S16), indicating negligible $^1O_2$ generation. Interestingly, under US irradiation, **Mn1** and **Mn2** consistently reduced methylene blue's absorbance (between 650–700 nm) (Figures 2d and S17), indicating their ·OH generation capacity. Control experiments conducted in the presence of **Mn1/Mn2** without US exposure indicated the necessity of US for ·OH generation (Figures S18 and S19). Furthermore, exposing methylene blue alone to the US did not affect its absorbance (Figure S20), confirming that the generation of ·OH required both ultrasound and the complexes. Although Mn(I)-tricarbonyl complexes are known for $^1O_2$ generation under light, this is the first time ·OH production is observed with any Mn(I)-tricarbonyl. Thus, these complexes might show sonotoxicity via the combined effects of $^1O_2$ and ·OH generation and CO release.

### DFT and TDDFT Calculation

DFT and TDDFT calculations were performed to understand the complexes' excited state chemistry.[22,23] Energy was calculated in water using the CPCM implicit solvation model.[22,23] The optimized structures matched well with the X-ray structure of **Mn2** (Figure S21), reflecting a distorted octahedral geometry around the Mn center. The frontier molecular orbitals (FMOs) of **Mn1/Mn2** revealed that the HOMO coincided with the Mn and, to some extent, at CO moiety (Figure S21). All complexes' LUMO was distributed on terpyridine moiety (Figure S21). This indicates the possibility of Mn(I)→terpyridine charge transfer in the complexes, as observed in their UV-vis absorption spectra. TD-DFT data revealed that the lowest transition energy from $S_0 \rightarrow S_1$ was 1.4 eV for **Mn2** and 2.46 eV for **Mn1** (Figure S22). Thus, the US dose of 1.0 MHz, 0.3 W cm$^{-2}$ can activate the complexes. Moreover, **Mn2** would be easily excited to $S_1$. The $\Delta E_{S0\text{-}T1}$ energy required for the conversion of $^3O_2$ to $^1O_2$ is 0.98 eV, and the calculated $\Delta E_{S0\text{-}T1}$ energy of **Mn1** and **Mn2** was 1.95 eV and 1.43 eV, respectively (Figure 3b), suggesting that these complexes can generate $^1O_2$ under US exposure.

### Cellular Toxicity

Based on the above-promising in-solution findings, we hypothesized that **Mn1** and **Mn2** hold promise as prospective US-responsive anticancer agents. Their anticancer efficacy was assessed against DL (Dalton Lymphoma cells) (Figures S23 and S24), MCF-7 (human breast cancer) (Figures S25 and S26) cancer cells, normal spleen cell (Figures S27 and S28), and human embryonic kidney (HEK-293) cells (Figures S29 and S30). under both, in absence or presence of US exposure (1.0 MHz, 0.3 W cm$^{-2}$) using the MTT assay.[10] In the dark (absence of US), **Mn1/Mn2** did not exhibit significant effects on cell viability (Figures S23, S24, S26, S28). However, under US exposure, **Mn1/Mn2** demonstrated concentration-dependent anticancer effects (Figures S23–S25, S27). The $IC_{50}$ values for **Mn2** against DL and MCF-7 cancer cells were *ca.* 0.54 ± 0.10 μM and 0.87 ± 0.06 μM, respectively (Figures S24 and S25, Table S3). In comparison, **Mn1** exhibited $IC_{50}$ values of 6.24 ± 0.61 μM and 4.18 ± 0.71 μM against these cell lines (Figures S23 and S25, Table S3). **Mn2** displayed approximately 12 times higher US-induced toxicity than its nonferrocene counterpart (**Mn1**), likely attributed to its lower excitation energy and higher $^1O_2$ quantum yield than **Mn1**. The ultrasound toxicity index (UI=Dark $IC_{50}$/US $IC_{50}$) of **Mn2** (13–16) was significantly higher than **Mn1** (UI = 1.4–2.0).

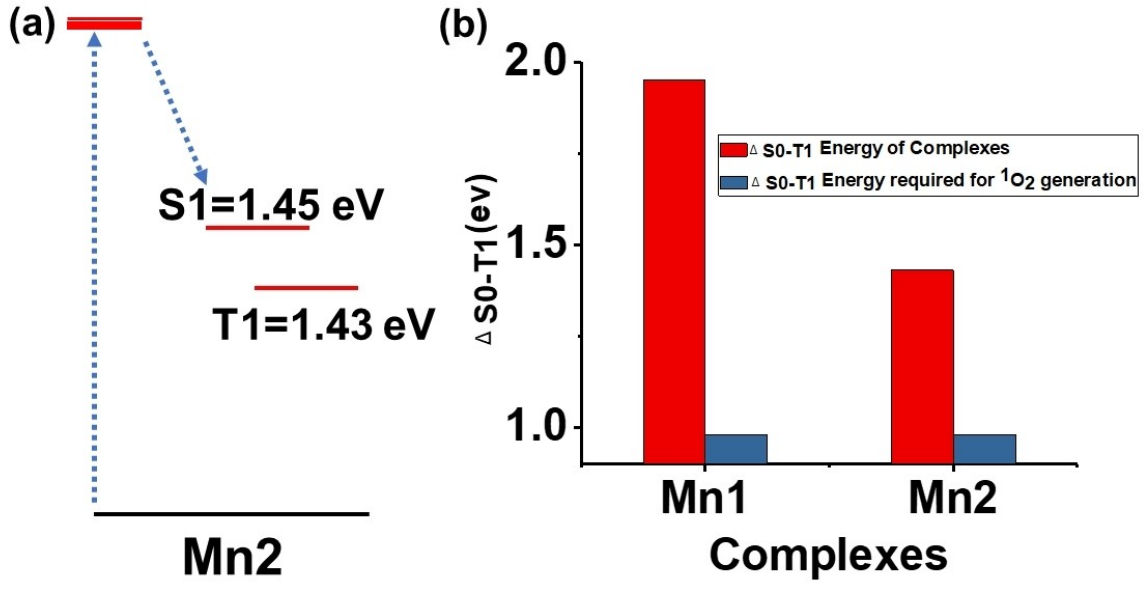


**Figure 3.** Calculated energy level of the ground, lowest excited singlet ($S_1$), and triplet ($T_1$) states of **Mn2**. (b) Adiabatic ground state – triplet state energy gap ($\Delta E_{S0-T1}$) of **Mn1** and **Mn2**.

These results indicated that incorporating the ferrocenyl moiety substantially enhances the sonocytotoxicity of the Mn(I) tricarbonyl complex. Similar observations were reported by Patra and coworkers where ferrocene conjugation to Ru(II)/Pt(II) complexes improves cytotoxicity (in the dark).[24] It is worth mentioning that this is the first time US-induced cytotoxicity is achieved with any Mn complex. Due to the lack of literature, comparison with the exciting literature is impossible at this stage. **Mn1**/**Mn2** did not exhibit significant toxicity towards spleen cells and HEK-293 cells (Figures S27–S30), indicating their initial biosafety. These findings underscore that under US exposure, **Mn2** selectively kills cancer cells with a high selectivity index (SI=Dark $IC_{50}$ in normal cells/US $IC_{50}$ in cancer cells) of 6–41. These findings highlight the potential of the first 3d metal-based (Mn-tricarbonyl) sonosensitizers for SDT.

### In-Cell ROS Generation and Depolarization of Mitochondria

As previously discussed, exposure of **Mn2** to the US enables the generation of $^1O_2$ and ·OH, suggesting its capacity to generate ROS via sonosensitization pathways (like type-I and type-II in PDT) in cancer cells.[24,25] To assess the intracellular ROS generation by **Mn2**+US in DL cancer cells, DCFDA (2,7-dichlorodihydrofluorescein diacetate) was used as an intracellular ROS marker.[26–28] In this assay, generated ROS catalyzes the oxidative conversion of nonfluorescent DCFDA to highly fluorescent DCF.[26–28] As illustrated in Figure 4a, **Mn2**+US treatment significantly enhanced intracellular ROS within DL cells, as indicated by intense intracellular green fluorescence in the **Mn2**+US-treated group. Importantly, minimal ROS generation was observed in the only **Mn2**-treated group (Figure 4a), affirming the safety profile of the complex. Importantly, only US exposure also did not cause an elevation of intracellular ROS (Figure 4a). Flow cytometry data further revealed that **Mn2**+US treatment resulted in approximately an 8-fold increase in ROS generation compared to the control and a 4-fold increase compared to **Mn2** alone (Figure 4b). Although Mn(I)-tricarbonyl complexes are reported for in-cell ROS production under light,[19] this is first-time in-cell ROS generation obtained with the US.

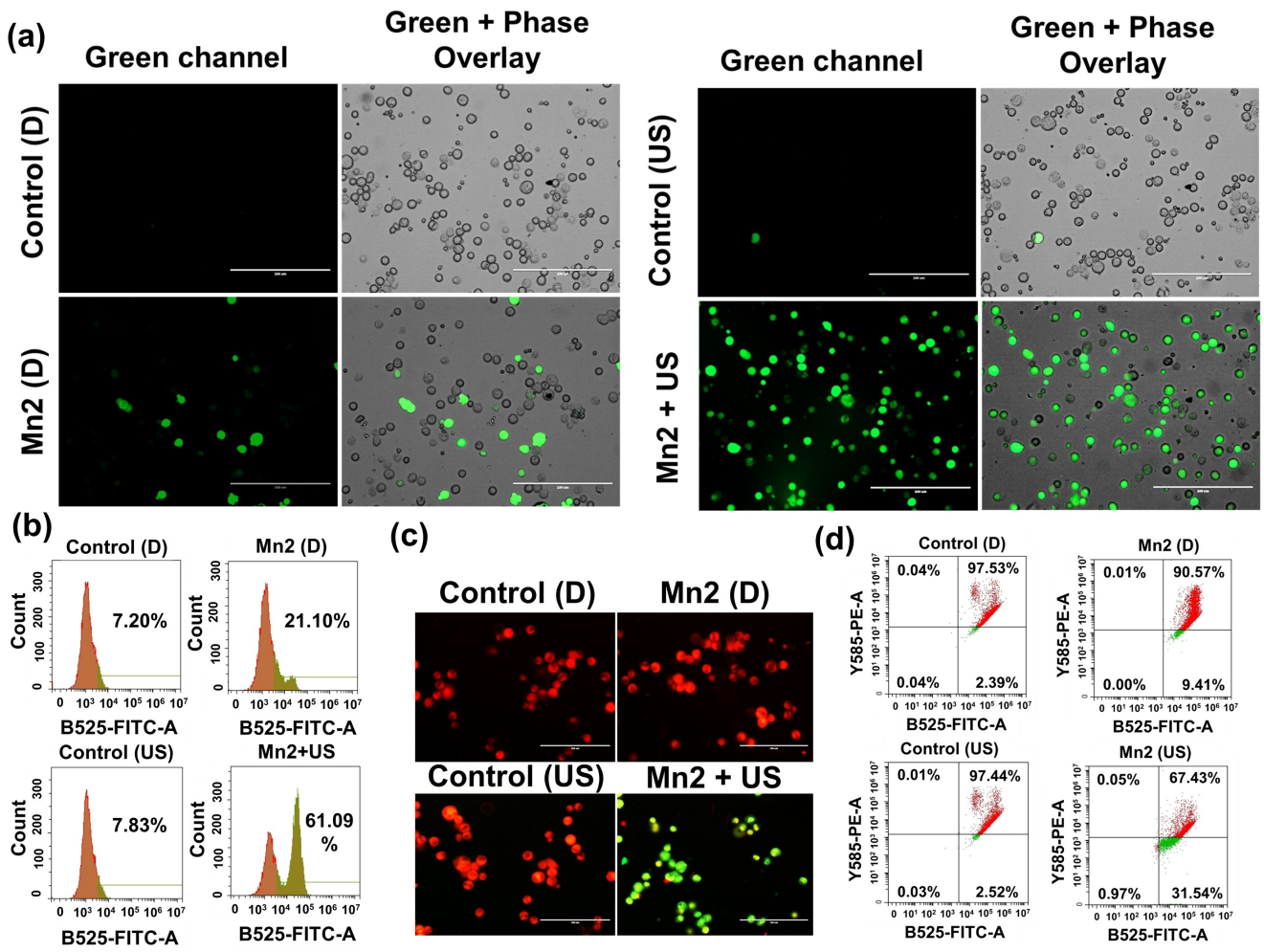


**Figure 4.** (a) Intracellular ROS generation in DL cells induced by **Mn2** under exposure of US (1.0 MHz, 0.3 W cm$^{-2}$) using DCFDA probe. Scale bar: 200 μm. (b) Quantitative detection (using flow cytometry) of intracellular ROS generated by **Mn2** and ultrasound. (c) Change in MMP of **Mn2** treated DL cells as monitored by JC-1 assay, scale bar: 100 μm. (d) Quantitative detection (by flow cytometry) of MMP change induced by **Mn2** and ultrasound.

Previous studies have suggested that metal complexes capable of inducing ROS and CO release influence mitochondrial membrane potential (MMP) effectively and initiate apoptosis in cancer cells.[29] Therefore, the impact of **Mn2** + US on the MMP of DL cells was visualized by a JC-1 assay.[29–31] In this method, JC-1 dye accumulates within the mitochondria and produces red fluorescence "J-aggregates" at high MMP, while diffusing in the cytoplasm as green fluorescent monomers at lower MMP.[29–31] As depicted in Figure 4c, **Mn2**-treated DL cells displayed a red fluorescence under dark conditions, indicating no significant alteration in MMP. However, upon US exposure, **Mn2**-treated DL cells demonstrated green fluorescence, suggesting a sudden drop and change in MMP. This data indicates that the **Mn2** + US combination effectively altered MMP, most likely due to effective ROS generation and CO release.[13,14] Furthermore, **Mn2**-induced MMP depolarization was quantitatively evaluated using flow cytometry (Figure 4d). As depicted in Figure 4d, MMP depolarization in the control groups was negligible. However, in the presence of **Mn2** + US, MMP decreased to 67%, significantly lower than **Mn2** alone (91%) (Figure 4d), implying again that **Mn2** had potent US-cytotoxicity and negligible dark cytotoxicity.

### Cell Death Pathways

The acridine orange (AO) and ethidium bromide (EB) staining were used to investigate the mode of cell death.[32] AO permeates all cells, staining nuclei green while EB enters only into dead cells with compromised membrane integrity, staining nuclei.[32] Thus, live cells exhibit normal green nuclei (due to AO staining), early apoptotic cells show bright green or yellowish-orange nuclei with condensed or fragmented chromatin, late apoptotic cells display condensed and fragmented orange-red chromatin, and cells undergoing necrosis exhibit structurally intact deep orange nuclei.[32] As shown in Figure 5a, DL cells treated with **Mn2** or US only displayed intact nuclear membranes, organized cytoplasm, and green nuclei, indicating their healthy nature.[32] However, after treatment with **Mn2** + US, DL cells exhibited bright green, yellowish-orange, and red nuclei indicative of early apoptosis, late apoptosis, and necrosis, respectively. Such kind of cell death might be related to immunogenic apoptosis.[33] Flow cytometry study was further carried out for quantitative determination of apoptosis.[34] A similar trend was observed in quantitative flow cytometry assessments. As illustrated in Figure 5b, the **Mn2** and US control group showed negligible cell death. In contrast, **Mn2** + US treatment resulted in approximately 23% early apoptosis, 42% late apoptosis cells, and 11% necrosis. Overall, these results again confirm that **Mn2** had potent US cytotoxicity and negligible dark cytotoxicity. These findings thus clearly indicate that **Mn2**-induced necro-apoptotic cell death via ROS-triggered mitochondrial depolarization.

### Caspase 3/7 Activation

A critical process in apoptosis is caspase activation.[35] Caspase activation in DL cells in the presence of **Mn2** and US was studied by caspase 3/7 and SYTOX staining.[35,36] Green fluorescence measured the active caspase in cells, while SYTOX uptake indicated apoptotic cells.[35,36] The results demonstrated that **Mn2** + US significantly activated caspase 3 (Figure 5c), indicating that this combination triggered the expression of the final executor of apoptosis, caspase 3, thereby facilitating cancer inhibition. Flow cytometry data also suggested activation of caspase 3 in the presence of **Mn2** + US (Figure 5d). These findings thus clearly indicate that **Mn2**, under US, induced apoptotic cell death via ROS-triggered mitochondrial depolarization and caspase 3 activation. Overall, the above results confirm that **Mn2** had potent US cytotoxicity and negligible dark cytotoxicity.

## Conclusions

In summary, we have successfully synthesized and characterized two US-sensitive terpyridine-based Mn(I) tricarbonyl complexes, **Mn1** and **Mn2**. **Mn2** is a novel bimetallic Mn(I) tricarbonyl complex, which was also characterized by X-ray diffraction. In **Mn2**, ferrocene was conjugated to lower the $S_0 \rightarrow S_1$ and $\Delta E_{S0\text{-}T1}$ energy gap, as shown by TDDFT calculation. **Mn2**, with a lower $S_0 \rightarrow S_1$ and $\Delta E_{S0\text{-}T1}$ energy gap than **Mn1**, showed better US-triggered $^1O_2$ and ·OH generation than **Mn1**. Importantly, this is the first time ROS generation was achieved with Mn(I) tricarbonyl complexes under US excitation. Moreover, again, for the first time, US-activated CO release (observed by myoglobin method and IR spectroscopic studies) was observed with these complexes. These complexes did not release CO or generate notable ROS without the US. These unprecedented in-solution (aqueous) results indicated the potential of **Mn1** and **Mn2** in sonodynamic therapy and CO gas therapy. Remarkably, the in-solution chemistries were translated to *in vitro* cellular models. **Mn1** and **Mn2** demonstrated minimal dark toxicity towards T-cell lymphoma (DL) and human breast cancer (MCF-7) cells while exhibiting significant necro-apoptotic cell death upon ultrasound (US) exposure via ROS and CO-mediated depolarization of mitochondria. Thus, any 3d metal complex showed sonodynamic therapy for the first time. The US-triggered cytotoxicity increased with the degree of conjugation, following the **Mn2** > **Mn1** trend. **Mn2**'s cytotoxicity under US exposure ($IC_{50} < 1\ \mu M$) surpassed that of previously reported with Re(I) based sonosensitizers.[9,11,14] **Mn1** and **Mn2** did not exhibit significant toxicity towards normal spleen cells, underscoring their tumor-selective anticancer potential. Overall, this study, for the first time, reported ultrasound-triggered CO release, ROS generation, and anticancer activities of any 3d metal complex.

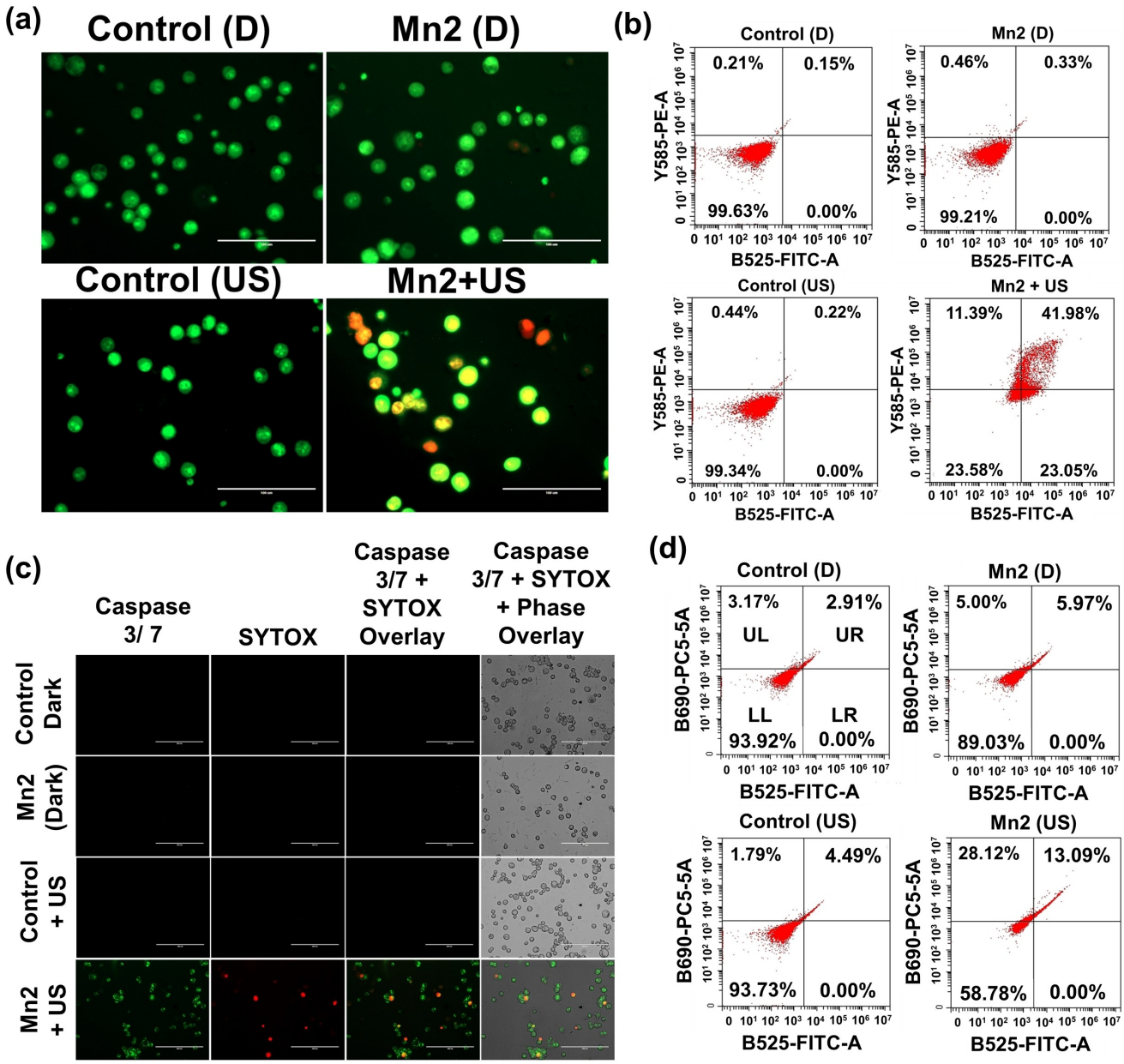


**Figure 5.** (a) AO and EB dual staining of DL cells collected from the control group (D), Control (US), **Mn2** (D), and **Mn2** + US. Scale bar: 100 μm. (b) Quantitative determination of mode of cell death by **Mn2** using flow cytometry. (c) Fluoroscence images showing Caspase 3/7 activation in DL cells induced by **Mn2** under exposure of US (1.0 MHz, 0.3 W cm$^{-2}$). Scale bar: 200 μm. (d) The apoptotic cells were detected with cell event Caspase-3/7 Green Detection Reagent and SYTOX red. Here, the Upper Left (UL) shows dead cells (Only SYTOX positive), the Lower Left (LL) represents live cells, the Lower Right (LR) quadrant shows only caspase 3/7 positive cells, and the Upper Right (UR) shows Caspase 3/7 positive + SYTOX Positive cells.

**Associated Content**

## Supporting Information Summary

Synthetic procedures, Methods, Tables for crystallographic data, Tables for $IC_{50}$ values, FMO energies, singlet – singlet transition energies, and adiabatic singlet – triplet splitting energies; figures for characterization data ($^1$H and $^{13}$C NMR, FT-IR, and HRMS), unit cell packing, photostability, FMOs, cell viability from MTT assay, $^1O_2$ and ·OH generation, Myoglobin assay.

Deposition number https://www.ccdc.cam.ac.uk/services/structures?id=doi:10.1002/chem.202403454 (for **Mn2**) contain the supplementary crystallographic data for this paper. These data are provided free of charge by the joint Cambridge Crystallographic Data Centre and Fachinformationszentrum Karlsruhe Access Structures service.

## Author Contributions

S. B. designed the studies and formulated the concept and overall project. A. K. Y., S. A., and R. K. synthesized and characterized the complexes. A. K. Y. did all the in-solution chemistry. S.S. and A.D. performed the SC-XRD measurements. V.S. and B.K. performed the biological assays. A. K. Y. performed the DFT and TD-DFT calculations. The manuscript was written with contributions from all authors. All authors have approved the final version of the manuscript.

## Acknowledgements

We thank the Royal Society of Chemistry (R23-4623502753) for financial support. A. K. Y and R. K. thank the Ministry of Education, the Government of India, for the Prime Minister's Research Fellowship. B. K acknowledges Banaras Hindu University for the financial support under the IoE scheme (File no. R/DEV/D/IoE/Incentive/2021-22/32449) and IoE SRICC Banaras Hindu University for Credit-Research Incentive for Faculty Members (SI. No. 361). We sincerely thank Ashish Kumar Maurya for his support during this work.

## Conflict of Interests

The authors declare that they have no known competing financial interests or personal relationships that could have appeared to influence the work reported here. SB, AKY, and RK have filed an Indian patent application (202411074006) lodged with the IIT (BHU) based on the novel composition and chemical structures reported here.

## Data Availability Statement

The authors confirm that the data supporting the findings of this study are available within the article and its SI. The raw data supporting this study's findings are available from the corresponding authors upon reasonable request.

**Keywords:** Sonodynamic Therapy · Sonosensitizer · Mn(I)-Tricarbonyls · Sonocytotoxicity · CO release

[1] S. C. Marker, A. P. King, R. V. Swanda, B. Vaughn, E. Boros, S. B. Qian, J. J. Wilson, *Angew. Chem. Int. Ed.* **2020**, *59*, 13391.
[2] S. Imstepf, V. Pierroz, R. Rubbiani, M. Felber, T. Fox, G. Gasser, R. Alberto, *Angew. Chem. Int. Ed.* **2016**, *55*, 2792.
[3] B. Kar, U. Das, N. Roy, P. Paira, *Coord. Chem. Rev.* **2023**, *474*, 214860.
[4] R. D. Rimmer, A. E. Pierri, P. C. Ford, *Coord. Chem. Rev.* **2012**, *256*, 1509–1519.
[5] J. Rossier, J. Delasoie, L. Haeni, D. Hauser, B. R. Rutishauser, F. Zobi, *J. Inorg. Biochem.* **2020**, *209*, 111122.
[6] G. Bag, D. Musib, M. K. Raza, A. Castonguay, M. Roy, *Polyhedron* **2024**, *249*, 116778.
[7] B. Neuditschko, A. P. King, Z. Huang, L. Janker, A. Bileck, Y. Borutzki, S. C. Marker, C. Gerner, J. J. Wilson, S. M. Meier-Menches, *Angew. Chem. Int. Ed.* **2022**, *61*, e202209136.
[8] A. E. Pierri, A. Pallaoro, G. Wu, P. C. Ford, *J. Am. Chem. Soc.* **2012**, *134*, 18197–18200.
[9] a) Y. Zhang, X. Zhang, H. Yang, L. Yu, Y. Xu, A. Sharma, P. Yin, X. Li, J. S. Kim, Y. Sun, *Chem. Soc. Rev.* **2021**, *50*, 11227–11248; b) G. Liang, T. Sadhukhan, S. Banerjee, D. Tang, H. Zhang, M. Cui, N. Montesdeoca, J. Karges, H. Xiao, *Angew. Chem. Int. Ed.* **2023**, *62*, e202301074.
[10] C. Li, Y. Pang, Y. Xu, M. Lu, L. Tu, Q. Li, A. Sharma, Z. Guo, X. Y. Sun, *Chem. Soc. Rev.* **2023**, *52*, 4392–4442.
[11] a) W. A. Velema, W. Szymanski, B. L. Feringa, *J. Am. Chem. Soc.* **2014**, *136*, 2178–2191; b) A. A. Mandal, R. Kushwaha, A. K. Yadav, S. Banerjee, *ChemBioChem* **2023**, *24*, e202200597.
[12] Y. Xu, Y. Pang, L. Luo, A. Sharma, J. Yang, C. Li, S. Liu, J. Zhan, Y. Sun, *Angew. Chem. Int. Ed.* **2024**, *63*, e202319966.
[13] a) J. Zhu, A. Ouyang, J. He, J. Xie, S. Banerjee, Q. Zhang, P. Zhang, *Chem. Commun.* **2022**, *58*, 3314–3317; b) A. K. Yadav, N. Kumar, A. T. Khan, R. Kushwaha, S. Banerjee, *ChemMedChem* **2022**, *17*, e202100615.
[14] R. Kushwaha, V. Singh, S. Peters, A. K. Yadav, T. Sadhukhan, B. Koch, S. Banerjee, *J. Med. Chem.* **2024**, *67*, 6537–6548.
[15] S. G. Gallego, G. J. L. Bernardes, *Angew. Chem. Int. Ed.* **2014**, *53*, 9712–9721.
[16] B. Kawahara, L. Gao, W. Cohn, J. P. Whitelegge, S. Sen, C. Janzen, P. K. Mascharak, *Chem. Sci.* **2020**, *11*, 467–473.
[17] L. Li, X. Yang, *Oxid. Med. Cell Longev.* **2018**, *2018*, 7580707.
[18] I. Chakraborty, S. J. Carrington, G. Roseman, P. K. Mascharak, *Inorg. Chem.* **2017**, *56*, 1534–1545.
[19] O. A. L. Rojas, B. Carvalho, R. Cabral, M. Silva, S. Friães, C. R. Rodrigues, M. S. H. Meireles, C. S. B. Gomes, J. A. A. Fernández, S. F. Vila, J. A. Rubiolo, L. Sanchez, P. V. Baptista, A. R. Fernandes, B. Royo, *J. Biol. Inorg. Chem.* **2022**, *27*, 49–64.
[20] T. Entradas, S. Waldron, M. Volk, *J. Photochem. Photobiol. B.* **2020**, *204*, 1117.
[21] A. Y. Satoh, J. E. Trosko, S. J. Masten, *Environ. Sci. Technol.* **2007**, *41*, 2881–2887.
[22] M. E. Casida, *Elsevier* **1996**, *4*, 391–439.
[23] Z. Fan, J. Xie, T. Sadhukhan, C. Liang, C. Huang, W. Li, T. Li, P. Zhang, S. Banerjee, K. Raghavachari, H. Huang, *Chem. Eur. J.* **2022**, *28*, e202103346.
[24] M. Manikandan, S. Gadre, S. Chhatar, G. Chakraborty, N. Ahmed, C. Patra, M. Patra, *J. Med. Chem.* **2022**, *65*, 16353–16371.
[25] F. Heinemann, J. Karges, G. Gasser, *Acc. Chem. Res.* **2017**, *50*, 2727–2736.
[26] Q. Yao, J. Fan, S. Long, X. Zhao, H. Li, J. Du, K. Shao, X. Peng, *Chem* **2022**, *8*, 197–209.
[27] Y. Pang, Q. Li, J. Wang, S. Wang, A. Sharma, Y. Xu, H. Hu, J. Li, S. Liu, Y. Sun, *Angew. Chem. Int. Ed.* **2024**, *63*, e202415802.
[28] K. M. Knopf, B. L. Murphy, S. N. MacMillan, J. M. Baskin, M. P. Barr, E. Boros, J. J. Wilson, *J. Am. Chem. Soc.* **2017**, *139*, 14302–14314.
[29] K. Kuang, C. Li, F. Maksut, D. Ghosh, R. Vinck, M. Wang, J. Poupon, R. Xiang, W. Li, F. Li, Z. Wang, J. Du, M. P. T. Fichou, G. Gasser, S. Bombard, T. Jia, *J. Biomed Sci.* **2024**, *31*, 50.
[30] K. Laws, G. B. Todd, A. Eskandari, C. Lu, N. O. Reilly, K. Suntharalingam, *Angew. Chem. Int. Ed.* **2018**, *57*, 287–291.
[31] J. Zhao, Y. Gao, R. Huang, C. Chi, Y. Sun, G. Xu, X. H. Xia, S. Gou, *J. Am. Chem. Soc.* **2023**, *145*, 11633–11642.
[32] A. Paul, P. Singh, M. L. Kuznetsov, A. Karmakar, M. F. C. G. da Silva, B. Koch, A. J. L. Pombeiro, *Dalton Trans.* **2021**, *50*, 3701–3716.
[33] H. Huang, S. Banerjee, K. Qiu, P. Zhang, O. Blacque, T. Malcomson, M. J. Paterson, G. J. Clarkson, M. Staniforth, V. G. Stavros, G. Gasser, H. Chao, P. J. Sadler, *Nat. Chem.* **2019**, *11*, 1041–1048.
[34] C. M. Che, R. W. Y. Sun, W. Y. Yu, C. B. Ko, N. Zhu, H. Sun, *Chem. Commun.* **2003**, 1718–1719.
[35] S. A. Lakhani, A. Masud, K. Kuroda, G. A. Porter, Jr, C. J. Booth, W. Z. Mehal, I. Inayat, R. A. Flavell, *Science* **2006**, *311*, 847–851.
[36] G. M. Buller, J. A. Bradford, J. Liu, W. L. Godfrey, *Blood* **2006**, *108*, 3879.

Manuscript received: September 20, 2024
Accepted manuscript online: November 6, 2024
Version of record online: November 26, 2024